Acta Geodaetica et Geophysica (2025) 60:97–114
https://doi.org/10.1007/s40328-024-00459-6

ORIGINAL STUDY

Ring current local time dependence during geomagnetic storms using equatorial Dst-proxies

Santiago Pinzon-Cortes[1,2] · Natalia Gómez-Pérez[3] · Santiago Vargas Domínguez[4]

Received: 2 July 2024 / Accepted: 26 November 2024 / Published online: 19 March 2025

Abstract
In this paper, we calculate Local Disturbance indices (LDi) using data from two equatorial observatories (Ascension ASC and Fúquene FUQ) to use them as Disturbance Storm-time (Dst) index proxies. We find that the LDi response to geomagnetic storms is different depending on the observatory's local time at the storm onset. In order to explore this local time influence on the measurements on the ground at low latitudes, we build new proxies using two observatories located at approximately the same longitude, in order to balance measurements in the north and south averaging meridional and measuring only zonal variations. The average of the longitude pairs and Dst-index proxies from single observatories exhibit strong correlation to the Dst index (≥ 0.88) during active periods and a moderate correlation (≤ 0.5) during quiet periods. We find that the storm intensity is associated with local time. We confirm that the fastest variation in the geomagnetic field during the storm is recorded between dusk and midnight, while the region between dawn and noon records more moderate variations, sometimes missing the storm effects altogether. Our results show an azimuthal asymmetry of the magnetospheric ring current, becoming most intense on the night side of the dusk terminator during active periods. We propose a new configuration for local time Dst proxies including the use of equatorial observatories. This will get insights of the evolution of storms in an area where there are limited geomagnetic observatories.

Natalia Gómez-Pérez and Santiago Vargas Domínguez have contributed equally to this work.

Extended author information available on the last page of the article

Graphical abstract

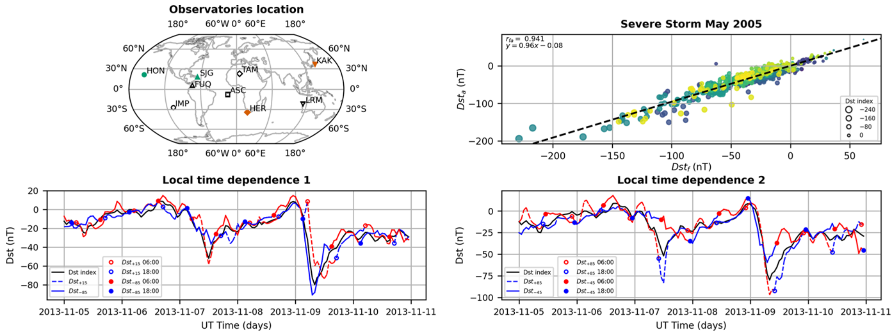

Keywords Dst index. Ring current asymmetry. Geomagnetic storms

1 Introduction

A geomagnetic storm is a disturbance in the electric and magnetic fields surrounding the Earth. These storms alter the amplitude and variability of the fields measured at Earth's surface, often leading to a decrease in the strength of the geomagnetic field at low latitudes. This occurs due to the interaction between the solar wind and the geodynamo, which generates the magnetosphere. During a geomagnetic storm, energy from the solar wind is

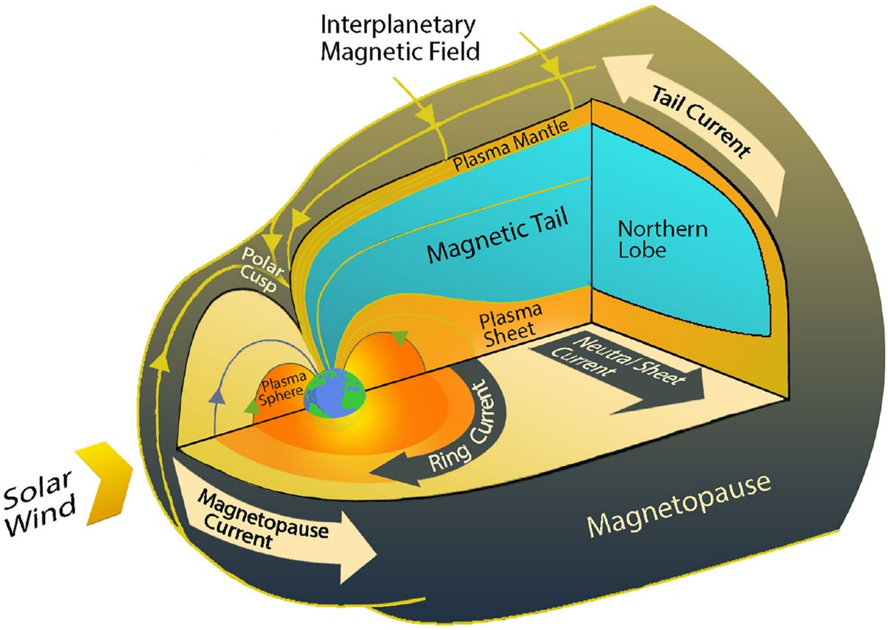

Fig. 1 Three-dimensional cross-section of the Earth's magnetic field with its currents and plasma regions: Modified from Kivelson and Russell (1995)

transferred to the magnetosphere as a consequence of the magnetic reconnection between the Interplanetary Magnetic Field (IMF) and the Earth's magnetic field. This interaction generates an enhancement of the Ring Current, which leads to a decrease of the horizontal component of the Earth's magnetic field at the equator (e.g., Gonzalez et al. 1994; Cramer 2013; Heilig 2018).

The ring current (RC) has been defined as a toroidal shaped current flowing on the equatorial plane of Earth (see Fig. 1), between 2 to 9 Earth radii (Daglis 1999). The RC flowing westward will oppose Earth's internal dipole and weaken the magnitude of the dipolar field measured at Earth's surface. During geomagnetic storms the variations measured on this dipolar component are mainly related to variations in the intensity of the flow in RC. There are two main current systems in this region at quiet times: an inner RC flowing westward, and an outer RC flowing Eastward above $3R_E$ (e.g. Ganushkina (2018)). These RC current systems are mostly symmetric during quiet times, but it has been observed they have an enhanced asymmetry during storm time. The nature of the magnetosphere is asymmetric, due to the direction of the solar wind: there is a compression of magnetic fieldlines on the dayside and and extension on the night side. This naturally results in a day-night asymmetry.

During storm time, charged particles from the tail are transported through the inner magnetosphere to the day-side magnetopause (Ganushkina 2018). A partial ring current that connects with the ionosphere is developed to balance the large input of charged particles transported in the night side plasma sheet into the inner magnetosphere. This partial ring current develops a strong westward current on the equatorial plane, that follows the fieldlines pole-ward at dusk and equator-ward at dawn. This results in large azimuthal dusk-dawn asymmetry on the RC during the main phase of a storm.

The Disturbance Storm-Time (Dst) index is traditionally used to quantify the perturbation of the axisymmetric RC. The Dst is correlated to the strength of the RC. The index is calculated by measuring the variation of the Horizontal (H) component of Earth's geomagnetic field at the equator (e.g., Heilig 2018). The Dst index was introduced by Sugiura

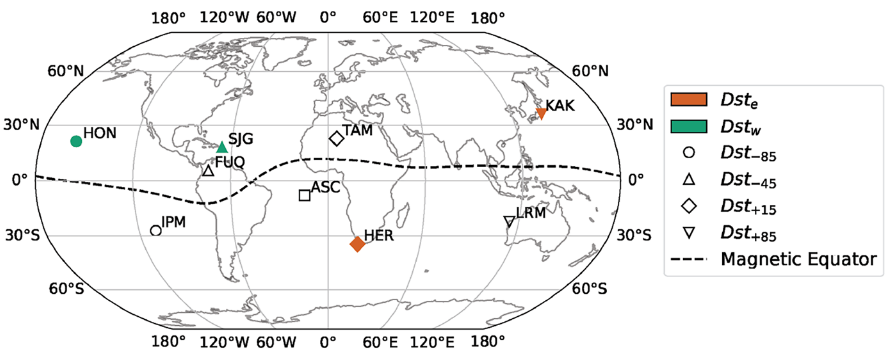

Fig. 2 Location of the observatories used in this study and their relative distance to the magnetic equator. The black dashed line corresponds to the magnetic equator calculated with IGRF13 (Alken et al. 2021). Observatories in orange correspond to east Dst index proxy Dst_e. Observatories in green correspond to the west Dst index proxy (Dst_w). The circle represents the observatories used in the Dst index proxy with mean local time UTC −8.5 (Dst_{-85}). The triangle up represents the observatories used in the Dst index proxy with mean local time UTC −4.5 (Dst_{-45}). Diamond represents the observatories used in the Dst index proxy with mean local time UTC +1.5 (Dst_{-15}).The triangle down represents the observatories used in the Dst index proxy with mean local time UTC +8.5 (Dst_{+85}). The square corresponds to the Ascension Island observatory

(1964) as a way to categorise geomagnetic storms by quantifying their strength (Sugiura 1991). The Dst index is calculated based on the hourly means of the horizontal component of the magnetic field measured at four mid-latitude observatories, i.e. Kakioka (KAK), Japan; Hermanus (HER), South Africa; Honolulu (HON), Hawaii; and San Juan (SJG), Puerto Rico (see Fig. 2). These locations are distributed in the northern and southern hemispheres to capture the signal from the RC and to have a complete local time coverage. These observatories are located at mid-latitudes, where the ionospheric and equatorial electrojet (EEJ) influences are not dominant. The Dst index is calculated and distributed by the World Data Center for Geomagnetism Kyoto and and dates back to 1957.

Magnetic storms are recorded as deep negative dips in the Dst index. Gonzalez et al. (1994) proposed a range of intervals for which the Dst minima characterises magnetic storm: weak (-30 nT to -50 nT), moderate (-50 nT to -100 nT), strong (-100 nT to -200 nT), severe (-200 nT to -350 nT) and great (< -350 nT).

The methodology for the calculation of the Dst-index (Sugiura 1991) has been expanded by different authors throughout the years. Love (2009) proposed the $\mathrm{Dst}^{5807-4SH}$ as a revised version of the Dst index. They first identify and remove active periods and replace them with interpolated values. These authors remove the solar-quiet (Sq) variation using a filter applied over time and frequency domains. Then, they filter the signals with frequencies that correspond to Earth's rotational and orbital periods; Moon's orbital period; as well as Moon-Earth coupling. Later, Gannon (2011) introduced 1-minute resolution data instead of the traditional hourly means.

Similarly, Iyemori (1990) introduced the Symmetric Disturbance index (SYM-H). This index uses the Horizontal component of ten observatories with latitudes ranging between −33.73° to 42.52°, although most of the observatories are in the northern hemisphere. The SYM-H uses 1-minute resolution data and has regular local time coverage.

Cid (2013) developed the Local Disturbance index (LDi) by using the Sugiura (1991) methodology, but applied it to data from a single observatory. They studied a list of the large magnetic storms dating back 1857, by calculating the LDi for the Colaba Observatory and the Alibag Observatory (ABG), Bombay.

Predictions of the Dst index based on statistical and computational methods can be found in the literature (for a recent review see Nair (2023)). Most models use solar wind data and prior Dst index as prediction parameters. Cristoforetti (2022) predict the Dst index using the three components (B_x, B_y, B_z) of the Interplanetary Magnetic Field; the solar wind plasma temperature, speed, density and pressure; and Dst index. They developed a model using Deep Learning Neural Network. Furthermore, they show the relevance of making a proper selection of the training data set to improve the prediction results.

Several authors have used the Dst index to study different mechanisms and characteristics of Earth's magnetic field. Echer (2008) compared the Dst index to interplanetary parameters (e.g. solar wind composition) from the Advance Composition Explorer spacecraft (ACE) to study 11 large storms. The authors were looking for triggering mechanisms for these large storms. They discovered there is a correlation between the electric field measured at L1 and the Dst-index. Their results indicate that the time-integrated energy from the solar wind is the most important parameter for determining the magnitude of a geomagnetic storm.

Soares (2020) used the Dst index to study the evolution through time of the geomagnetic field measured at Tatuoca (TTB) and analysed the effects on these measurements from the Equatorial Electrojet (EEJ). They show a time analysis from 1957 to 2019, where the measurements at the observatory are influenced by its proximity to EEJ, which is measured by the magnetic dip angle. Their results exhibit an increment in the range of the horizontal component over time that highlights the transition of the daily variation from the Sq (Solar quiet) type to EEJ type. Also, seasonal variations and daily variations were larger during the period of EEJ influence.

Balan et al. (2014, 2016) argued that Dst index does not capture completely the severity of storms. Instead, they proposed the mean value of the Dst index during the main phase (Dst_{MP}) as a better indicator of storm severity. They showed that Dst_{MP} is better correlated with the disruption in electrical power services and damage.

Newell and Gjerloev (2012) proposed four ring current indices. The indices are calculated as the SYM-H, but using 98 mid and low-latitude observatories from the SuperMAG collaboration. The indices are called SMR-00, SMR-06 SMR-12 and SMR-18, where the number of each index represents the central local time. By using the partial indices, they found storm intensity differences associated with local time; SMR-18 (dusk) exhibits more intense storms, while SMR-06 (dawn) exhibits less severe storms. They conclude that the intensity difference represents an asymmetry in the Ring Current during the main phase of the storms. Also, the ring current returns to its symmetrical state during the recovery phase of the storms.

Yakovchouk et al. (2012) calculate global and local Dxt index to study the properties of several storms of different intensities. Dxt index follows the same methodology proposed by Sugiura (1991), but the local disturbances are normalized by the cosine of station's geomagnetic latitude. Their findings revealed that the minima of the local Dxt index are 25% to 30% deeper than those of the global Dxt index. Moreover, they observed that the most significant disturbance occurs around 18:00 local time. As a result, they concluded that the global Dxt index underestimates the severity of disturbances, emphasizing the utility of the local Dxt index in studying both the spatial distribution and temporal evolution of storms.

In this paper, we want to study the geomagnetic storms and how they develop on ground based on local time. Methods and data section describes the methodology, data sources, and information about the observatories used in this study. Results and discussion section provides the analysis in two main parts: First, we calculate Dst index proxies at low latitude observatories, analogous to the LDi, using the data from the Geomagnetic Observatory of Fúquene (FUQ), Colombia and the Ascension Island Observatory (ASC), Atlantic Ocean. Second, we propose a Local Time distribution array, to analyse the dependence of the disturbance over the Earth's geomagnetic field with the local time. Lastly, in the Conclusions we explain the advantages of using LDi to identify and classify storms and how LDi shows a correlation between storm intensity and local time at the storm commencement.

2 Methods and data

A good part of our analysis uses Local Disturbance indices (LDi), Cid (2013). They are calculated using the methodology proposed by Sugiura (1991) for a single observatory as follows:

- Take the hourly mean of the horizontal (H) component measured at the ground observatory. Calculate and extract the annual quadratic tendency, $H_{base}(t)$, using the mean of the five international quiet days of each month, published by World Data (2023). This correction accounts for the geomagnetic secular variation:

$$\Delta H(t) = H_{obs}(t) - H_{base}(t) \tag{1}$$

where $H_{obs}(t)$ correspond to the horizontal component measured at the observatory.

- Calculate and extract the Solar quiet (Sq) variation by taking the five international quiet days of each month and extracting the daily variation frequency for $m_{max} = 3$ and $n_{max} = 3$,

$$Sq(t,s) = \sum_m \sum_n A_{mn} \cos(mt + \alpha_m) \cos(ns + \beta_n) \tag{2}$$

where t represents the local time and s the month number; and

- Apply a magnetic latitude correction to normalize the index:

$$LDi(t) = \frac{D(t)}{cos(\phi)} \tag{3}$$

where $D(t) = \Delta H(t) - Sq(t,s)$, and ϕ is the dipole latitude of the observatory. ϕ estimation is based on the current IGRF; see Table 1. Data from observatories presented in this paper was downloaded from Instituto Geografico Agustin Codazzi (IGAC) (1953-2024); INTERMAGNET (1991-2020); World Data Cente for Geomagntism (2003-2020)

2.1 Equatorial local disturbance indices

The Dst index is obtained by averaging LDi of KAK, HON, HER, and SJG observatories. The name, IAGA code, location, and dipole latitude of the observatories used in this study are summarized in Table 1.

First, we produce two LDi using data from FUQ and ASC (Dst_f and Dst_a respectively). We calculate and compare the correlation between Dst_f, Dst_a, and the Dst index.

We re-calculate two new proxies and define them as east and west, Dst_e and Dst_w respectively, by calculating the LDi for two stations and averaging them. For Dst_e we use KAK and HER, and for Dst_w we use HON and SJG observatories. See Fig. 2 for the observatories locations and Table 1 for the observatories information. We quantify the linear correlation between proxies with the Pearson Correlation coefficient.

Table 1 Observatories name, IAGA code, location, and dipolar latitude (Lat_{dip}). The geomagnetic coordinates are determined using model calculations provided by the British (2023)

Observatory	IAGA code	Geographic coordinates	Lat_{dip} (2005-2010)
Fúquene	FUQ	5.47ºN 286.263ºE	15.78
Ascension Island	ASC	7.949ºS 345.624ºE	−2.33
Kakioka	KAK	36.232ºN 140.186ºE	27.36
Honolulu	HON	21.320ºN 202.000ºE	21.65
Hermanus	HER	34.424ºS 19.225ºE	−33.99
San Juan	SJG	18.111ºN 293.85ºE	20.36
Easter Island	IPM	27.171ºS 250.59ºE	−18.87
Learmonth	LRM	22.220ºS 114.100ºE	−32.45
Tamanrasset	TAM	22.790ºN 5.530ºE	24.67

Table 2 The first column corresponds to the proxy name. The second column shows the pair of observatories used (see also Fig 2). The third column is the local time average between the observatories

Proxy	Observatories	Local time (UTC)
Dst_f	FUQ	−05:00
Dst_a	ASC	00:00
Dst_e	KAK - HER	+05:00
Dst_w	HON - SJG	−07:00
Dst_{-85}	HON-IPM	−08:30
Dst_{-45}	SJG-FUQ	−04:30
Dst_{+15}	HER-TAM	+01:30
Dst_{+85}	KAK-LRM	+08:30

We use data from Instituto Geografico Agustin Codazzi (IGAC) (1953-2024); INTERMAGNET (1991-2020); World Data Cente for Geomagntism (2003-2020). In the case of FUQ, we had had to apply some baseline corrections combining the absolute measurements and the variometer measurements in record.

2.2 Local time proxies

We construct an array of observatories for the intensity of the ring current that varies with the local time and generate LDi for several observatories and then average them in pairs (see Fig. 2). When using the pairs we define the local time by averaging the local time of the observatories used (see Table 2).

3 Results and discussion

3.1 The Dst and equatorial local disturbance indices

In order to study how the LDi correlates with Dst-index, we selected 6 periods of time of one-month length with different geomagnetic activities: two Severe storms in May 2005 and June 2015; one Strong storm in July 2004; one Moderate storm in October 2013; and two Quiet time on August 2008 and October 2014. All the correlation coefficients between various proxies are summarized in Table 3.

3.1.1 Severe storms

Figure 3 shows the results for the month of May 2005. We observe that during that time there are 3 geomagnetic storms. Two of them correspond to strong storms (between the 7th and the 11th; and after 28th) and one to a severe storm (between the 15th and the 23rd). Figure 3A shows that Dst_f and Dst_a capture the main features of the storms. There is a high correlation (> 0.93) between the proxies and the Dst-index (Table 3).

We found a good correlation between all the proxies we constructed (> 0.88) (see Table 3). However, there is a higher correlation for Dst_f with Dst_w than for Dst_f with Dst_e. In Figs. 3B, D we observe the correlation with Dst_f has the largest magnitude during the main

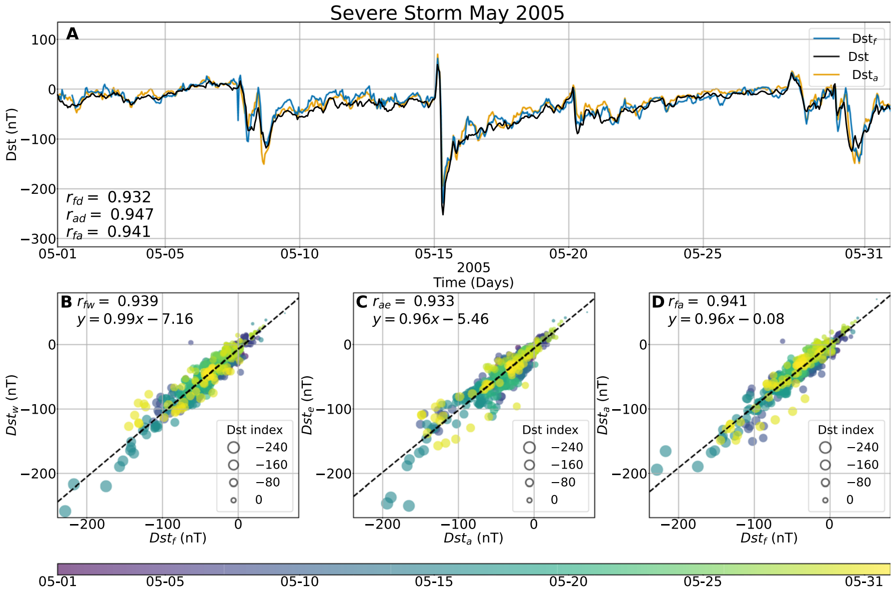

Fig. 3 Comparison and correlation of Dst index proxies for the Severe storm in May 2005. A) Comparison between Fuquene LDi (Dst_f; blue line), Ascension LDi (Dst_a; yellow line) and Dst-index (black line). At the top left there is the Pearson correlation coefficient between Dst_f and Dst-index (r_{fd}); Dst_a and Dst-index (r_{ad}); and Dst_f and Dst_a (r_{fa}). B-D) Scatter plots between various proxies throughout the severe storm. Each Figure shows the correlation for each hourly-mean value of the proxy. In color, we show the corresponding date in 2005. The size of the dots shows the value of the Dst index. The correlation coefficient is shown on the top left corner and the dashed line shows the best-fit line and its equation is shown in the top left corner. These series show how the correlation is relatively good except for the storm time. Each proxy captured the minimum value at slightly different times and different minimum values. In B and D we see Dst_f has minima larger (i.e. shallow dip) than expected from other proxies associated with local time

phase of the severe storm (aquamarine blue dots). The discrepancy in correlation is observed mainly during strong storms (purple and yellow). We found that Dst_a in ASC exhibits similar behavior, but this proxy is more closely related to Dst_e (see Figure 3C, see Table 3).

We observe a parallel between Dst_f with Dst_w and Dst_a with Dst_e correlations related to the intensity recorded by each proxy. This suggests that there might be a local time influence, where Dst_f is better represented by Dst_w because the contribution of SJG data over Dst_w, that has a similar local time as FUQ. Likewise, Dst_a is similar to Dst_e because the HER contribution presents a similar local time with ASC.

Figure 4 shows the proxies during the month of June 2015. The main storm occurred between June 22nd and June 26th and is classified as Severe. There is a high correlation between Dst-index and the proxies (> 0.9) (see Table 3). The Dst_a minimum occurs a few hours before Dst-index. However, Dst_f and Dst_a capture the main features of the Dst index as well as the storm behavior (see Fig 4A).

Figures 4 B-D show that the correlations are weaker at the main phase of the storm (shown in green). Also, the correlations r_{fw} and r_{ae} are the higher proxies correlations (≥ 0.92)(see Table 3). This exhibits the local time influence where Dst_f is similar to Dst_w and Dst_a is similar to Dst_e because of similarities in local time. The r_{ae} correlation is worse during the storm, and it is caused by the time difference of the minima (see Fig. 4C).

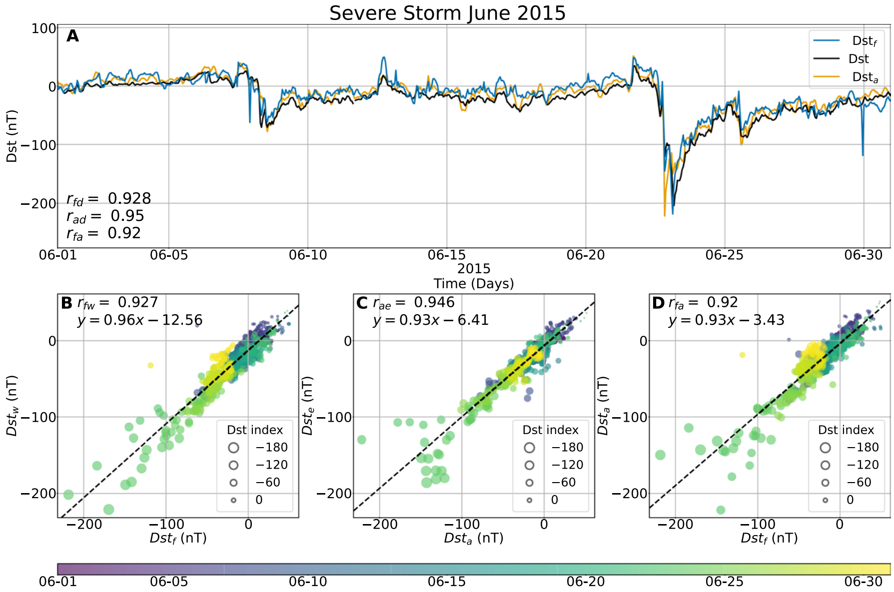

Fig. 4 Same as Fig. 3 but for the Severe storm in June 2015. This severe storm exhibits a more complex behavior and this results in worse proxy correlation indices. The spread in the scatter plot is larger during the storm time for each of the cases shown here than in Fig. 3. In B and C, we see that Dst$_f$ and Dst$_a$ show more intense storms

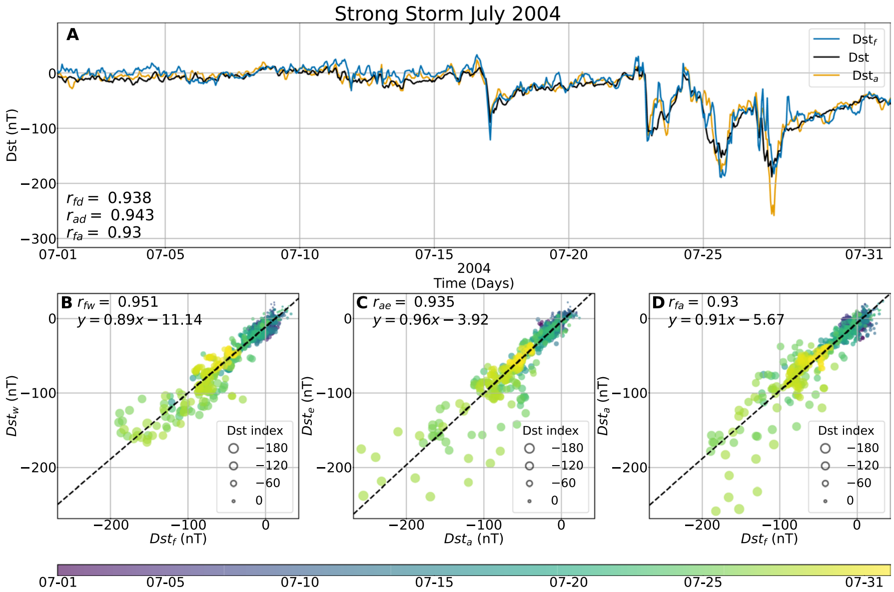

Fig. 5 Same as Fig. 3 but for the Strong storm in July 2004. This storm can be separated into clear sections with storm min and recovery when another is superimposed. The correlation indices worsen but all proxies capture the three stages clearly

3.1.2 Strong storms

We observe a strong geomagnetic storm between July 22nd to August 1st, 2004 (Fig 5). This storm is a multiphase storm that presents several local minima. Figure 5A shows Dst_f and Dst_a exhibit the multiple steps of the storm as Dst-index. The proxies and Dst-index correlation is high (>0.88) (see Table 3).

The weakest correlation occurs during the multiple Dst-index minima of the storm (green to yellow dots) (see Fig. 5 B–D). r_{fw} and r_{ae} are the largest correlations and exhibit the correspondence between Dst_f with Dst_w and Dst_a with Dst_e (see Fig 5 B, C). However, Fig. 5 B, D show a slope less than 1 of best-fit lines. This indicates a difference in the rate of change between the proxies, possibly associated with the multiphase behavior.

3.1.3 Moderate storms

During October 2013, we identify 3 moderate geomagnetic storms (Fig. 6). Dst_f and Dst_a record the 3 storms and capture the main features (Fig. 6A). During this period the correlation of the proxies and the Dst-index decreases to moderate (> 0.73). Dst_f and Dst_a exhibit more intense main phase minima. We observe that all correlations are worse during the quiet time and the recovery phase of the storms (see Fig. 6 B–D). Also, the slopes of the best-fit lines are less than 1. This indicates a difference in the variations captured by each proxy. However, r_{fw} and r_{ae} still exhibit the highest correlations that support a local time effect in the proxies.

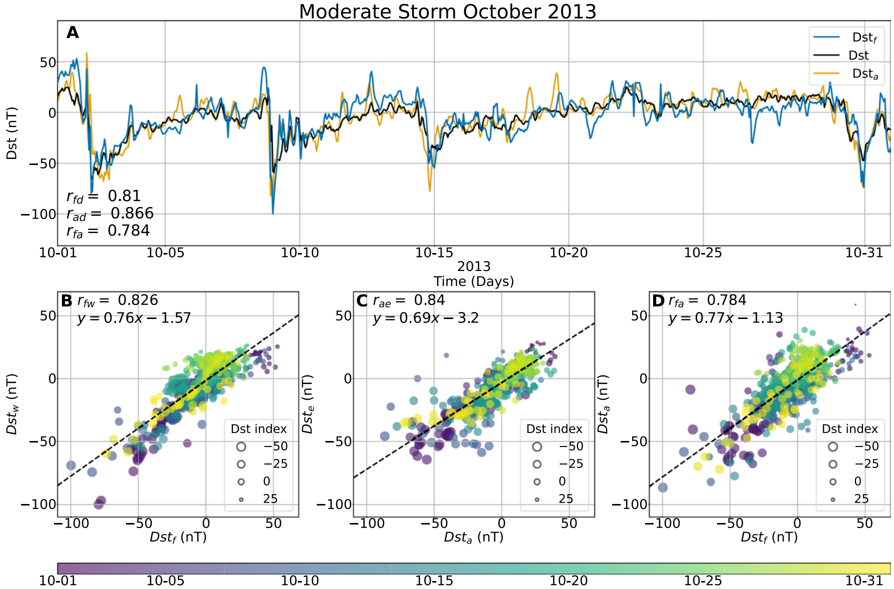

Fig. 6 Same as Fig. 3 but for the Moderate storm in October 2013.Moderate storms show a worse correlation than severe storm data. The correlation is also worse during the quiet time in this time series

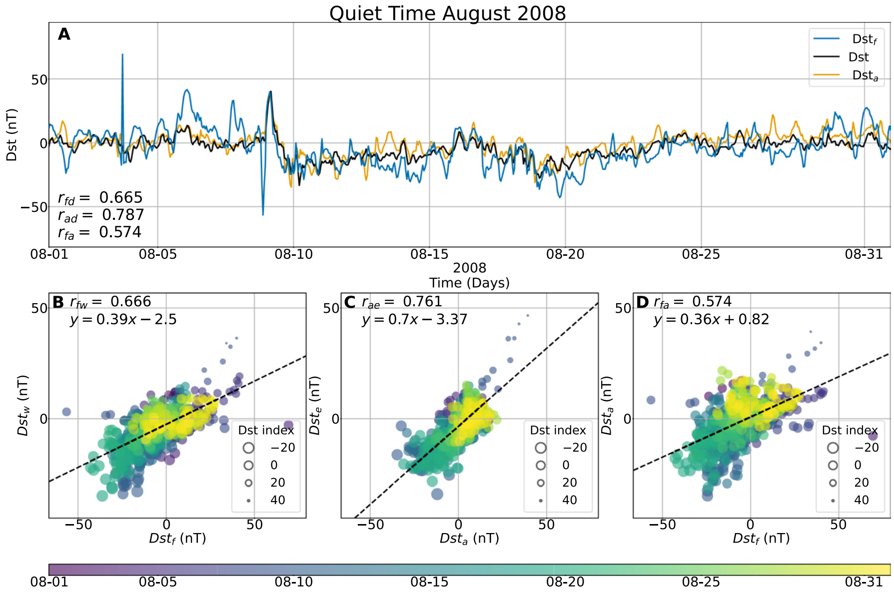

Fig. 7 Same as Fig. 3 but for the Quiet time in August 2008

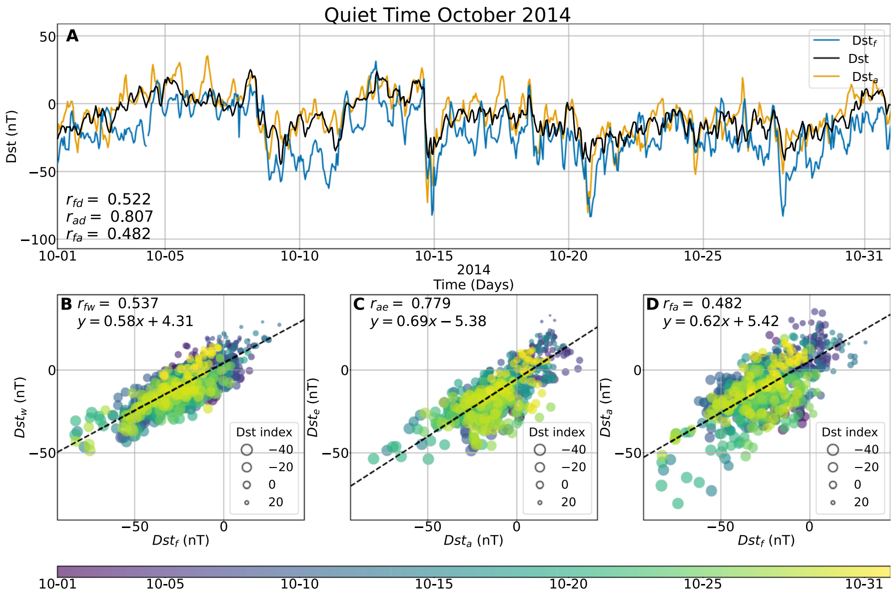

Fig. 8 Same as Fig. 3 but for the Quiet time in October 2014

Table 3 Pearson Correlation Coefficient of each period studied and the storm classification

July, 2004 (Strong storm)				May, 2005 (Severe Storm)				August, 2008 (Quiet time)			
	Dst-index	Dst_f	Dst_a		Dst-index	Dst_f	Dst_a		Dst-index	Dst_f	Dst_a
Dst-index	1	0.938	0.943	Dst-index	1	0.932	0.947	Dst-index	1	0.665	0.787
Dst_f	0.938	1	0.930	Dst_f	0.932	1	0.941	Dst_f	0.665	1	0.574
Dst_a	0.943	0.930	1	Dst_a	0.947	0.941	1	Dst_a	0.787	0.574	1
Dst_e	0.976	0.880	0.935	Dst_e	0.979	0.886	0.933	Dst_e	0.935	0.580	0.761
Dst_w	0.975	0.951	0.905	Dst_w	0.981	0.939	0.922	Dst_w	0.941	0.666	0.718
October, 2013 (Moderate storm)				October, 2014 (Quiet time)				June, 2015 (Severe)			
	Dst-index	Dst_f	Dst_a		Dst-index	Dst_f	Dst_a		Dst-index	Dst_f	Dst_a
Dst-index	1	0.810	0.866	Dst-index	1	0.522	0.807	Dst-index	1	0.928	0.950
Dst_f	0.810	1	0.784	Dst_f	0.522	1	0.482	Dst_f	0.928	1	0.920
Dst_a	0.866	0.784	1	Dst_a	0.807	0.482	1	Dst_a	0.950	0.920	1
Dst_e	0.958	0.730	0.840	Dst_e	0.949	0.454	0.779	Dst_e	0.988	0.907	0.946
Dst_w	0.971	0.826	0.834	Dst_w	0.945	0.537	0.749	Dst_w	0.990	0.927	0.934

3.1.4 Quiet and unsettled geomagnetic environment

We study two periods of quiet time (Figs 7 and 8). The first one corresponds to August 2008 and the second one corresponds to October 2014. Dst_f and Dst_a records the quiet month behavior during each period. During this period, the proxies present more variations compared to the Dst index. Also, the correlation between the proxies and Dst-index ranges from medium to moderate (see Table 3).

r_{fw} and r_{ae} correlations as well as the slopes of best fit, do not support the local time influence observed during active periods. Also, r_{fa} correlation is the lowest in both periods of time (3). This shows that proxies from a single observatory do not capture the same features.

The lower value of the correlation suggests that during quiet periods the RC does not induce a significant field over ASC and FUQ. It is likely other currents, such as the Sq that has not been completely removed, play a more significant role during quiet periods.

3.2 Local time influence

In Figure 3B–D we observe that each proxy has a different minima during the storms. Dst_w and Dst_f have deeper minima than the other proxies during the severe storm (May 15th). The Dst-index minimum occurs at 08:00 UT, which coincides with the local time of Dst_w and Dst_f being close to midnight. In contrast, Dst_a has a shallower minimum and its local time is after dawn. This suggests that storm intensity is affected by the local time. This behavior is likewise present in Figures reffig:2015B-D. In this case, not only the intensity is different in each proxy, but also the time of the main storm.

Similarly, the decrease in the correlations in Figure 6B–D is associated with the difference in the intensity captured by each proxy. Regarding the intensity differences of each proxy in Fig. 6B–D, we observe that for the first storm Dst_w has the deepest minimum while Dst_e and Dst_a has the less intense main phase. This storm occurs at 07:00 UT, which indicates that Dst_w is close to midnight and Dst_e Dst_a are close to noon and dawn respectively. Similarly, the second storm in Fig. 6 occurs at 00:00 UT. Dst_f and Dst_a exhibit the more intense main phase and their local time is dusk and midnight respectively. At the third storm Dst_f and Dst_a exhibit the deepest values, while Dst_e exhibit the less intense storm. As Dst index records the storm at 23:00 UT, Dst_f and Dst_a local time is dusk and midnight respectively, and Dst_e local time is near dawn.

During the 2004 strong storm is not possible to determine if the intensity is dependent on the proxies' local time due to the multiphase behavior of the storm (see Fig. 5).

To study in detail the local time (LT) influence on storm intensity we constructed a local time array. We select the Dst index observatories (HON, SJG, HER, KAK) as principal observatories and select a secondary observatory in the same time zone as the principal observatory. The secondary observatories are Easter Island (IPM), Fúqune (FUQ), Tamanrasset (TAM), and Learmonth (LRM) (see Table 2 and Fig. 2).

Figure 9 shows two storms in 2013. Figures 9 A and B exhibit the period from July 4th through July 10th, 2013. Dst-index suggests a moderate storm with the main peak at the end of July 6th. Figure 9A shows how the storm starts at the same time for Dst_{-85} Dst_{+15} and Dst-index. However, Dst_{-85} reaches the storm maxima before the Dst-index. Also, Dst_{+15} reaches the storm maxima almost at the same time as Dst-index, which exhibit

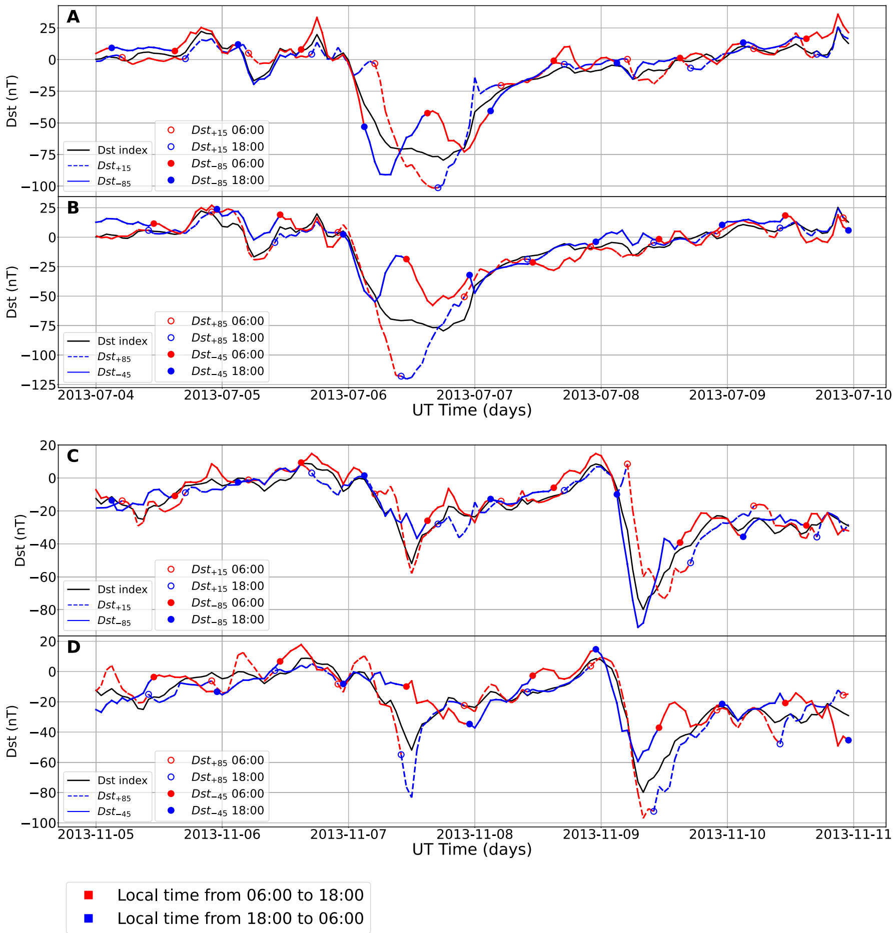

Fig. 9 Local time variation during two events from 2013. Their plot shows Dst-proxy versus UT time. Colour red represents Local Time from 06:00 to 18:00; blue represents Local time from 18:00 to 06:00. Black line: Dst-index. Open/filled red circle corresponds to 06:00 h local time; open/filled blue circle corresponds to 18:00 h local time; A-B) July 4th to 9th, 2013 event. A) solid line: proxy HON-IPM (Dst$_{-85}$) and dashed line: proxy HER-TAM pair (Dst$_{+15}$). B) solid line: proxy SJG-FUQ (Dst$_{-45}$) and dashed line: proxy KAK-LRM pair (Dst$_{+8.5}$). C-D) November 5th to 10th, 2013 event. C) solid line: proxy HON-IPM (Dst$_{-85}$) and dashed line: proxy HER-TAM pair (Dst$_{+15}$). D) solid line: proxy SJG-FUQ (Dst$_{-45}$) and dashed line: proxy KAK-LRM pair (Dst$_{+85}$). These graphs show how the local time affects the intensity of the storm. The deeper minima occur between dusk and midnight. During dawn and midnight, we see shallower minima

more intense storms than that recorded by Dst-index. Dst$_{-85}$ minima occur at night and Dst$_{+15}$ minima occurs at dusk. Figure 9B shows how Dst$_{+85}$ reaches the more intense values ($< -100nT$), but Dst$_{-45}$ does not capture the storm. Dst$_{+85}$ minima occur at dusk, while Dst$_{-45}$ is between dawn and noon during the storm's main phase.

Figures 9 C and D show the events from November 6th to November 10th, 2013. We observe two moderate storms during this time: on November 7th and 9th. Figure 9 C shows that Dst_{+15} and Dst_{-85} record both storms. During the first storm, Dst_{+15} and Dst-index main phase occurs at the same time and the minimum point represents almost the same intensity. Also, Dst_{-85} has a slight decrease but does not reach storm values. The Dst_{+15} minimum is at afternoon and Dst_{-85} minimum occurs at dawn. During November 9th storm, Dst_{+15} and Dst_{-85} have a similar behavior as Dst-index. Dst_{-85} exhibits a more intense storm than Dst-index, while Dst_{+15} records a less intense storm than Dst-index. Dst_{-85} minimum occurs after dusk and Dst_{+15} minimum occurs close noon.

Figure 9 D shows the Dst_{+85} and Dst_{-45} comparison with Dst-index. During November 7th storm, we observe that Dst_{+85} has captured the storm, but reaches more intense values (> -80 nT). On the other hand, Dst_{-45} does not record the storm. When the Dst-index minimum occurs, Dst_{-45} LT is at dawn. On the other hand, the Dst_{+85} LT is after dusk. At November 9th storm, both Dst_{-45} and Dst_{+85}, exhibit the storm features. Despite the fact that both proxies capture the storm, there is an important difference in the intensity of the storm. Dst_{-45} records a less intense storm than Dst-index at LT dusk and Dst_{+85} has a deeper minimum at LT dusk.

We find that the magnitude of the effects on Earth depend not only on the solar wind energy and density or magnetic field orientation, but also on the local time of the observatory while the storm develops. The areas most affected by a given geomagnetic storm are those between dusk and midnight during the onset and storm maxima. The geomagnetic storm is a global phenomena that induces rapid changes around the globe changing the geomagnetic environment rapidly, but we have found that the fastest changes around the equator occur on the night close to dusk, as a response to the intensifying ring current. Our results suggest that LDi indices can be used to characterize the influence of magnetic storms as localized events as well as identify regions of increased vulnerability during geomagnetic storms.

4 Conclusions

Geomagnetic storms can disturb operations and technology on ground (e.g. Boteler 2019; Mac Manus 2022) and space (Zheng et al. 2019). Their effects may destroy infrastructure and result in very costly consequences. In order to understand these effects scientists study the sun, the solar wind and its interaction with the geomagnetic field. In this work, we use geomagnetic observatory data to determine the influence of geomagnetic storms of various magnitudes on these observatory measurements, probing the equatorial geomagnetic environment.

We calculated the variation of the horizontal magnetic field component measured at equatorial observatories (LDi at ASC and FUQ), as well as matching local-time pairs of mid-latitude observatories.

The marked differences between pairs as well as the equatorial LDi measurements indicate that a global index, such as the Dst, is not enough to characterize the effect a geomagnetic storm may have at ground level, and it is necessary to develop a well-distributed equatorial field with comprehensive local time coverage to better characterize the influence on auroral regions that are susceptible to disturbances during geomagnetic storms.

With our results, we have shown that in order to assess in real time the geomagnetic variations at a specific location, when you do not have a local geomagnetic observatory, it is important to use a local time measurement of the geomagnetic field, instead of only relying on global indices (e.g. Kp, ap and Dst) which might underestimate the local conditions. Additionally, single equatorial observatory measurements are a good indicator of the equatorial ring current (both axisymmetric and asymmetric components) which is correlated to auroral oval expansion, and the increase in geomagnetic variability at higher latitudes (Yokoyama et al. 1998), where ground induced currents will be more damaging.

Our study extends the applicability of local Dxt indices proposed by Yakovchouk et al. (2012). By incorporating equatorial proxies we will add more insights that will help to understand the spatial distribution and temporal evolution of the storms. Geomagnetic observatories need a long time commitment of resources and funding. In order to have a sufficient local time coverage, it is necessary to guarantee the timely production of good quality data.

Acknowledgements The results presented in this paper rely on data collected at magnetic observatories. We thank the national institutes that support them and INTERMAGNET for promoting high standards of magnetic observatory practice (www.intermagnet.org). We acknowledge WDC Kyoto for providing Dst index hourly data and GFZ Potsdam for the International Quiet Days (IQD). We thank Daniela Hernández Beltrán, Orlando Rangel Pérez, Mayra Isabel Vargas Cáceres, Pamela Mayorga Ramos, and all the staff from Instituto Agustín Codazzi (IGAC) managing the geomagnetic Observatory for their help providing the FUQ data. We acknowledge Ciaran Beggan, Chris Turbitt, and BGS for their help in processing data. We acknowledge the Beyond Research program from Facultad de Ciencias, Universidad Nacional de Colombia. SP wishes to thank Juan Sebastián Ramirez-Rugeles for helpful conversations to develop the code. Special thanks to the anonymous reviewers for their invaluable feedback, which greatly improved this manuscript.

Author contributions SPC was responsible for data analysis, interpretation, and text editing. NGP contributed to data analysis, interpretation and text editing. SVD contributed to data analysis and text editing. All authors have thoroughly reviewed and approved the final manuscript.

Funding Open Access funding provided by Colombia Consortium. SVD is supported by 'Beyond Research Program', Facultad de Ciencias, Universidad Nacional de Colombia.

Availability of data and materials Geomagnetic Observatory of Fúquene datasets analyzed during this current study are available in the Instituto Geográfico Agustín Codazzi (IGAC) repository. Datasets analysed from other observatories can be obtained through the INTERMAGNET web site for datasets generated in this study contact the corresponding author.

Declarations

Conflict of interest The authors declare that they have no Conflict of interest.

References

Alken P, Thébault E, Beggan CD, Amit H, Aubert J, Baerenzung J, Zhou B (2021) International geomagnetic reference field: The thirteenth generation. Earth Planets Space 73(2021):1–25

Balan N, Skoug R, Ram ST, Rajesh PK, Shiokawa K, Otsuka Y, Nakamura T (2014) CME front and severe space weather CME front and severe space weather. J Geophys Res: Space Phys 11910(041–10):058. https://doi.org/10.1002/2014JA020151

Balan N, Batista IS, Ram ST, Rajesh PK (2016) A new parameter of geomagnetic storms for the severity of space weather A new parameter of geomagnetic storms for the severity of space weather. Geosci Lett 3:1

Boteler DH (2019) 10. A 21st century view of the March 1989 magnetic storm A 21st century view of the March 1989 magnetic storm. Space Weather 17:1427–1441

British Geological Survey (2023) Geomagnetic Coordinate Calculator. Geomagnetic coordinate calculator. https://geomag.bgs.ac.uk/data_service/models_compass/coord_calc.html, Last accessed on 2023-05-23

Cid C, Palacios J, Saiz E, Cerrato Y, Aguado J, Guerrero A (2013) 5. Modeling the recovery phase of extreme geomagnetic storms Modeling the recovery phase of extreme geomagnetic storms. J Geophys Res: Space Phys. https://doi.org/10.1002/jgra.50409

Cramer WD, Turner NE, Fok MC, Buzulukova NY (2013) Effects of different geomagnetic storm drivers on the ring current: CRCM results Effects of different geomagnetic storm drivers on the ring current: CRCM results. J Geophys Res: Space Phys. https://doi.org/10.1002/JGRA.50138

Cristoforetti M, Battiston R, Gobbi A, Iuppa R, Piersanti M (2022) Prominence of the training data preparation in geomagnetic storm prediction using deep neural networks Prominence of the training data preparation in geomagnetic storm prediction using deep neural networks. Sci Rep 12:127631

Daglis IA, Thorne RM, Baumjohann W, Orsini S (1999) The terrestrial ring current: Origin, formation, and decay The terrestrial ring current: Origin, formation, and decay. Rev Geophys 37:37407–438. https://doi.org/10.1029/1999RG900009

Echer E, Gonzalez WD, Tsurutani BT (2008) Interplanetary conditions leading to superintense geomagnetic storms ($Dst \leq -250nT$) during solar cycle 23. Geophys Res Lett. https://doi.org/10.1029/2007GL031755

Gannon JL, Love JJ (2011) USGS 1-min Dst index USGS 1-min Dst index. J Atmos Solar-Terr Phys. https://doi.org/10.1016/J.JASTP.2010.02.013

Ganushkina NY, Liemohn MW, Dubyagin S (2018) Current systems in the Earth's magnetosphere current systems in the Earth's magnetosphere. Rev Geophys 56:309–332. https://doi.org/10.1002/2017RG000590

Gonzalez WD, Joselyn JA, Kamide Y, Kroehl HW, Rostoker G, Tsurutani BT, Vasyliunas VM (1994) What is a geomagnetic storm? What is a geomagnetic storm? J Geophys Res 99:5771. https://doi.org/10.1029/93JA02867

Heilig B, Beggan C, Lichtenberger J (2018). Natural sources of geomagnetic field variations. Natural sources of geomagnetic field variations. Geneva, Switzerland. http://nora.nerc.ac.uk/id/eprint/523717/

Instituto Geografico Agustin Codazzi (IGAC) (1953-2024). Geomagnetic observatory data for FUQ. data retrieved from, https://www.colombiaenmapas.gov.co/observatoriotierrayterritorio

INTERMAGNET (1991-2020). Geomagnetic observatory data. data retrieved from Intermagnet, https://doi.org/10.5880/INTERMAGNET.1991.2020

Iyemori T (1990) Storm-time magnetospheric currents inferred from mid-latitude geomagnetic field variations Storm-time magnetospheric currents inferred from mid-latitude geomagnetic field variations. J Geomagn Geoelectr 42:1249–1265. https://doi.org/10.5636/JGG.42.1249

Kivelson MG, Russell CT (1995) Introduction to Space Physics Introduction to space physics. Cambridge University Press

Love JJ, Gannon JL (2009) Revised Dst and the epicycles of magnetic disturbance: 1958–2007 Revised Dst and the epicycles of magnetic disturbance: 1958–2007. Annal Geophys 27:3101–3131. https://doi.org/10.5194/angeo-27-3101-2009

Mac Manus DH, Rodger CJ, Dalzell M, RentonA Richardson GS, Petersen T, Clilverd MA (2022) Geomagnetically induced current modeling in New Zealand: extreme storm analysis using multiple disturbance scenarios and industry provided hazard magnitudes geomagnetically induced current modeling in New Zealand: extreme storm analysis using multiple disturbance scenarios and industry provided hazard magnitudes. Space Weather 20:e2022SW003320

Nair M, Redmon R, Young LY, Chulliat A, Trotta B, Chung C, Slavitt I (2023) MagNet–A data-science competition to predict disturbance storm-time index (Dst) from solar wind data magnet–a data-science competition to predict disturbance storm-time index (dst) from solar wind data. Space Weather 21:e2023SW003514

Newell PT, Gjerloev JW (2012) SuperMAG-based partial ring current indices Supermag-based partial ring current indices. J Geophys Res 117:5215

Soares G, Yamazaki Y, Cnossen I, Matzka J, Pinheiro KJ, Morschhauser A, Stolle C (2020) Evolution of the geomagnetic daily variation at Tatuoca, Brazil, From (1957) to 2019: a transition from Sq to EEJ. J Geophys Res: Space Phys. https://doi.org/10.1029/2020JA028109

Sugiura M (1964). HOURLY VALUES OF EQUATORIAL Dst FOR THE IGY Hourly values of equatorial Dst for the IGY. Ann. Int. Geophys. 35, https://www.osti.gov/biblio/4554034

Sugiura M, Kamei T, Berthelier A, Menvielle M (1991). Equatorial Dst index : 1957-1986 Equatorial dst index : 1957-1986. Saint-Maur-Des-Fosses

World Data Cente for Geomagntism (2003-2020). Geomagnetic observatory data. data retrieved from WDC, https://wdc.bgs.ac.uk/

World Data Center for Magnetism, Kyoto (2023). The international 5 and 10 quietest and 5 most disturbed days [1932 -]. https://wdc.kugi.kyoto-u.ac.jp/qddays/index.html, Last accessed on 2023-05-23

Yakovchouk OS, Mursula K, Holappa L, Veselovsky IS, Karinen A (2012) Average properties of geomagnetic storms in 1932–2009 Average properties of geomagnetic storms in 1932–2009. J Geophys Res 11:73201

Yokoyama N, Kamide Y, Miyaoka H (1998) The size of the auroral belt during magnetic storms The size of the auroral belt during magnetic storms. Annal Geophys 16:5566–573

Zheng Y, Ganushkina NY, Jiggens P, Jun I, Meier M, Minow JI, Kuznetsova MM (2019) Space Radiation and Plasma Effects on Satellites and Aviation: quantities and metrics for tracking performance of space weather environment models space radiation and plasma effects on satellites and aviation: quantities and metrics for tracking performance of space weather environment models. Space Weather 17:1384–1403

Authors and Affiliations

Santiago Pinzon-Cortes[1,2] · Natalia Gómez-Pérez[3] · Santiago Vargas Domínguez[4]

✉ Santiago Vargas Domínguez
svargasd@unal.edu.co

Santiago Pinzon-Cortes
pinzons@cua.edu

Natalia Gómez-Pérez
ngp@bgs.ac.uk

1 Physics Department, The Catholic University of America, 620 Michigan Ave NE, Washington, D.C., USA

2 Departamento de Geociencias, Universidad Nacional de Colombia, Carrera 45 No. 26-85, Bogotá, Colombia

3 Multi-hazards and Resilience, British Geological Survey, Research Avenue South, EH14 4AP, Edinburgh, UK

4 Observatorio Astronómico Nacional, Universidad Nacional de Colombia, Carrera 45 No. 26-85, Bogotá, Colombia